Acta Mechanica Slovaca **28 (1): 52 - 59,** March **2024**
https://doi.org/10.21496/ams.2024.015

Acta Mechanica Slovaca
ISSN 1335-2393
www.actamechanica.sk

Absorption Potential of Modern Steels when used for the Car-body Evaluated by the 3-point Bending Test with Stretching

Marek Buber [1,*], Emil Evin [1], Miroslav Tomáš [1]

[1] Department of Automotive Production, Faculty of Mechanical Engineering, Technical University of Košice, Mäsiarska 74, 040 01 Košice

Abstract: Beside the active safety components of the car, the passive safety elements incorporated in the car-body structure are important too. To ensure passenger safety during a car accident, advanced materials are used in deformation zones. The article deals with testing the material's absorption ability by a 3-point bending test with stretching. The test allows simulating material behaviour during bending load when combined with stretching and determining the properties of the metal sheets, such as the absorption potential of the material and stiffness constant. The purpose of this article is to evaluate the innovation potential of the dual-phase steel HCT600X and austenitic steel AISI 304, which are used in the automotive industry for body-in-white structural components, when compared to the drawing-quality steel DC05. By substituting cold-rolled steel DC05 with dual-phase steel HCT600X, the absorption potential increase about 2.01 at side impact and about 1.09 at frontal impact. Otherwise, when substitute cold-rolled steel DC05 with austenitic steel AISI 304, the absorption potential increase about 1.46 at side impact, and about 2.52 at frontal impact. It was found that the stiffness constant c evaluated at the bending test allowed determining the ability of material to absorb the impact energy at a short deformation path, which occurs in side impact during accident. Thus, in side deformation structures, it is better to use dual-phase steel HCT600X than austenitic steel AISI 304.

Keywords: 3-point bending test; energy absorption; deformation work; stiffness constant

1. Introduction

A large number of passive safety features have been replaced by electronically controlled active safety features. The efficiency of the braking system was improved by adding control units and the ABS system, which enabled better controllability of vehicles in critical situations [1]. The complete safety of passengers cannot be achieved either by connecting autonomous driving systems to the car or by using the function of control units that help to better control the vehicle. "Perfect" crew safety can only be achieved by ensuring the integrity and structural strength of the body-in-white. While standard drawing quality steels commonly used in the car-body perform good formability [2], advanced high strength steels are used in order to enhance the passenger's safety [3] due to high strength. Mihalikova tested dynamic behaviour of dual-phase steel [4], while Valeš et al presented the use of dual-phase steels for outer body panels [5]. The use of different types of steel in the car body can achieve high structural strength in places where it was necessary. In the past, an increase in strength had to be achieved by changing the thickness of the sheet metal used, resulting in an increase of weight and thus consumption [6].

Nowadays, the car body consists of different types of steel, which allows to reduce its weight through the application of high-strength steels in critical places and thus to

*** Corresponding author:** Marek Buber, ***E-mail address:*** *marek.buber@tuke.sk*

reduce the weight of the car body itself. For example, if in the past they wanted to increase the strength of the B-pillar, they had to proceed by changing the thickness of the material or using an additional layer of sheet metal [7]. While today it is sufficient to change the strength of the column using another high-strength steel, for example MART Steel, AHSS, or PHS, which makes it possible to continue or even reduce the thickness of the sheet metal [8]. The options will bring this weight of the bodywork and thus fuel savings [9], a smaller ecological impact on the environment and also a saving of the material used for the production of the car [10,11].

It was necessary to develop a body concept that would not only guarantee the safety of vehicle passengers but also pedestrians. Deformation zones and their correct location and design ensure the absorption of impact energy to a much higher extent than was the case in the past. When designing the body, it should not be forgotten that its front part should have a controlled course of deformation: 1. pedestrian protection. 2. protection at low speeds - parking manoeuvres; 3. compatibility - protection of a co-participant in a traffic accident; 4. self-protection - the necessity to observe biomechanical criteria; 5. crew survival space; (Fig. 1). [12]

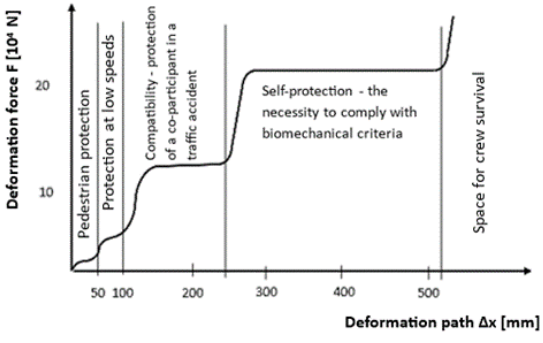

Figure 1: Progressive course of deformation in front collision [12].

Today's car-bodies are designed in such a way that in the event of a side impact where the space for deformation is very small, the absorption of a large amount of energy is ensured in a short deformation path. The opposite is the front and rear of the car, which, on the other hand, absorb the impact energy over a long distance during an impact, thus protecting the passengers from high acceleration [13]. Collision with a vehicle from the side is the most dangerous for the crew, therefore, high-strength modern materials are applied to the body's lateral reinforcements, which prevent the penetration of body parts into the cabin space [14].

Research of modern steels used in the body-in-white has a great importance from many points of view. Pednekar et al. [15] researched GEN3 advanced high strength steels when used for A and B-pillar parts of the car body. The increase in post-forming yield strength of GEN3 AHSS due to work and bake hardening contributes strongly toward crash performance in energy absorption and intrusion resistance. Rodríguez-Martínez et al. [16] researched AISI 304 steel and analysed its behaviour when subjected to perforation under a wide range of impact velocities. Due to transformation of austenite into martensite during mechanical loading, this process leads to an increase in strength and ductility of the material. Thus, makes this steel attractive for engineering applications, such as structural elements responsible for absorbing energy under fast loading. Cotterell et al [17] investigated the mechanical properties of the undeformed part of the sample after a tensile test. They found that there were changes in micro-hardness in the entire measured length of the sheet metal. However, the most deformed grains are in the sample with a rolling direction 0°. It follows that the strengthening of the material in the given area is also correlated with the size of the deformation. In the case of deep-drawing DC steels, where large deformation is expected both during the crash and during the forming of the part itself, deformation strengthening is useful and has an effect on the stiffness of the part made of this type of sheet metal. Sommer et al [18] focused on the dynamic deformation properties of austenitic stainless steel in a tensile test with deformation rates of 1000 s^{-1}. They investigated the distribution of deformation during the test using digital image correlation. They found that at such a high rate of deformation, pores appear in the structure of the material. They discovered that these pores could come directly from production, where dust particles or impurities were rolled into the material. An increased concentration of such "cavities" can cause a violation of the material in this area. New materials are applied also in a new gradual energy-absorbing structures, as Xu et al applied in subway vehicles [19]. They evaluated the energy absorption of the structure when verified the numerical simulation of the impact test by the experiment. Dual phase steels are applied in these deformation structures

due to high strain hardening exponent n values and high energy absorption of impact energy [20]. Larn and Yang studied the influence of different amounts (10, 20, and 40%) of compressive deformation of austenite on the subsequent isothermal transformation of bainite in Fe, Mn, Si, C alloy steels. The prior deformation of austenite had a strong impact on the bainitic transformation, because it created defects which hinder the growth of bainite and resulted in finer microstructure [21].

The article is focused to the research of absorption potential of dual phase steel HCT600X and austenitic stainless steel AISI 304 by the three-point bending test with stretching. As a reference material standard cold-rolled drawing quality steel DC05 was used. The fixture allows testing material absorption potential in combined bending and stretching conditions. This type of loading is typical for such car boy parts as beams, bumpers, roof and door reinforcements. By this test, the ability of material to absorb the impact energy at specified path can be measured and compared.

2. Materials and methodology of experiments

2.1 Materials and their properties

Metal sheets made of cold-rolled drawing quality steel DC05, dual-phase steel HCT600X (DP600) and austenitic stainless steel AISI 304 were used for the experiment. The chemical composition was measured by the spectrometer Belec Compact Port and it is shown in Tab. 1.

Tab. 2 shows the material properties of the investigated materials. The properties were evaluated in the 90° directions. The mechanical properties were determined by a tensile test according to STN EN ISO 6892-1 [22]. The normal anisotropy coefficients (Lankford coefficients) were determined according to STN EN ISO 10 113 [23]. The strain hardening exponent, and the material constant were determined according to STN EN ISO 10 275 [24].

2.2 Three-point bending test

The experiment was carried out under predetermined conditions such as the deformation speed, the deformation path and the force required to deform a sample with a width of 26 mm and a length before deformation $L_0 = 300$ mm (the length of the loaded part of the sample $L_0 = 2.X_0 = 2x110$ mm) and the thickness of the sample $a_0 = 0.75$ mm (Fig. 2).

The experimental test was carried out on a TIRAtest 2300 testing machine. Before experiment it was necessary to hold the sample in such a way

Table 1: Chemical composition of the experimental materials.

Material	Chemical composition %								
	C	Si	Mn	P	S	Cu	Al	Ni	Ti
DC5	0.03	0.01	0.18	0.009	0.010	-	0.044	0.003	0.002
HCT600X	C	Si	Mn	P	S	Cu	Al	Cr	Mo
	<0.111	0.279	1.963	0.026	<0.002	0.019	0.031	0.206	<0.002
	Ni	V	Ti	Nb	Co	W	Fe		
	<0.002	0.012	<0.002	0.02	0.017	<0.005	97.31		
AISI 304	C	Si	Mn	P	S	Cu	Al	Cr	Mo
	0.055	0.592	1.597	0.018	<0.002	0.029	0.009	18.30	0.015
	Ni	V	Ti	Nb	Co	W	Fe		
	7.79	0.040	0.007	0.049	0.062	0.015	71.42		

Table 2: Mechanical properties of the experimental materials.

Material	Proof strength $R_{p0.2}$ [MPa]	Tensile strength R_m [MPa]	Uniform ductility A_g [%]	Ductility A_{80} [%]	Strength constant K [MPa]	Strain-hardening exponent n [-]	Plastic strain ratio r [-]	Strain offset φ_0 [-]
DC05	166	280	27	49	502	0.241	1.90	0.0081
HCT600X	371	627	19.3	30.7	1095	0.220	0.81	0.0053
AISI 304	305	750	61	67	1614	0.491	1.01	0.0316

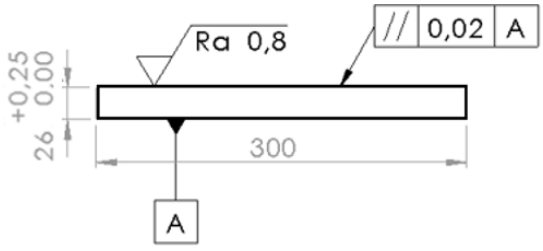

Figure 2: Dimensions of the tested sample.

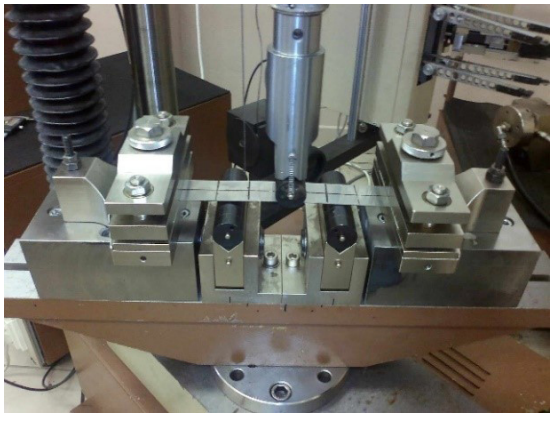

Figure 3: Three-point bending test [25].

that it would not move from the holder during the test. The sample was stressed by three-point bending and the forces were measured using a loading-cell mounted on the machine punch. In the case of three-point bending, it is possible to stress the sample by combined bending and stretching. The distance travelled and the loading force were recorded by the computer. The supporting rollers placed to support the sample were 110 mm apart and their diameter was $d = 30$ mm (Fig. 3). The samples were tested in two conditions: 1-until fracture (long deformation path); 2-on bending punch path 25 mm (short deformation path). Test were performed on 3 specimens for each material and average value and standard deviation was calculated.

2.3. Methodology of experiment evaluation

After the bending test, based on the punch path and geometrical proportions (see Fig. 4), such characteristics as specimen elongation and its springback were evaluated. These characteristics were evaluated at the punch path of 25 mm in order to reach the maximum strain before the neck occurs, and the individual quantities were as follows: h - bend path; h' - path of the bender after unloading force; α' - angle after unloading force; α''- angle under load; X_0' - length of half of the examined part of the sample in the unloaded state; X_0'' - length of half of the examined part of the sample under load.

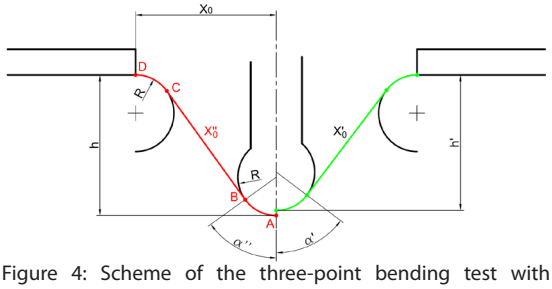

Figure 4: Scheme of the three-point bending test with stretching.

The specimen's elongation was calculated based on relations (1) and (2). It is assumed that the specimen's free length is deformed uniformly depending on the bending path h until the neck occurs. In the initial position of the bender $h = 0$, the length of the sample was 110 mm. Then, the angle α can be expressed as follows:

$$\alpha(h) = -2.tang^{-1}\left(\frac{x_0 - \sqrt{h^2 - 4.r.h + x_0^2}}{h - 4.r}\right), \qquad (1)$$

when adding the arc length AB and CD and adding the free length BC, the half of the specimen's length x after deformation is calculated as follows:

$$x = 2\frac{\pi.\alpha.r}{180} + \frac{x_0}{\cos(\alpha)} - 2.r.\tan(\alpha), \qquad (2)$$

then, the total length of the specimen is double of the x obtained from equation (2).

The deformation work, i.e., the energy absorption of the steel [19], was evaluated from the course of bending punch force on the bending punch path at two levels: at the punch path of 25 mm and at the point of maximum bending force (thus, the bending punch path at the point of the fracture) as follows:

$$W_{def} = \int_{x=0}^{x_{max}} F(x) \cdot dx \cong \sum_{i=1}^{n} \overline{F}_i \cdot \overline{x}_i. \qquad (3)$$

The stiffness constant c can be determined from the record of the bending force Fmax depending on the path of the bending punch x_{max}. When the linear course of the force-path dependence is assumed, the stiffness constant c will represent the direction of the straight line indicated in the dependence, as it is shown in Fig. 5. The fit factor was within the

punch path 0 to material fracture.

3. Results and Discussion

Based on the bending test scheme shown in Fig. 4 and relations (1) and (2), the angles during loading and unloading and the total length of the sample were calculated, the values of which are given in Tab. 3.

The length of the free part of the sample in the loaded state, with the travelled path of the bending punch of 25 mm for the reference steel DC 05, was 121.75 mm. After the sample was unloaded, the material contracted by 1.31 mm, which was 1.11 mm less than that of the HCT600X steel and 1.2 mm less than that of the austenitic steel AISI 304. The force required to deform the sample by 25 mm reached a value of 5.201 kN for the reference steel DC 05, which was half as much as for the HCT600X steel, where the force reached a value of 10.453 kN. For AISI 304 steel it was 7.619 kN, which was 2.418 kN more than the reference steel.

Test were performed on 3 specimens for each material and average value and standard deviation was calculated. The deformation work Wdef needed to deform the sample until the moment of its fracture reached the value of 246.3±1.6 J for the reference steel DC05. The similar deformation work needed to deform the sample was for the HCT600X steel and reached the value of 269.6±2.1 J. For the AISI 304 steel, the force needed to deform the sample was 2.5 multiplied and reached the value of 620.1±3.5 J. The deformation work Wdef 25mm needed to deform the sample on path 25mm reached the value 130.7±2.0 J for HCT600X steel and that was more than twice like for deforming reference material. For AISI 304 deformation work reached 95.3±2.8 J and that was only one and half more than for deforming reference material.

On Fig. 6 is a comparison of the deformation work at the three-point bending test with stretching (Tab.4). $W_{def\ 25mm}$ represents the work required to deform sample on path 25 mm by bending punch. Wdef,max represents the work required to deform the sample until failure in three-point bending with stretching. According to the graph, we can conclude that the material AISI 304 is able to absorb the largest amount of energy in three-point bending with stretching. However, when bending at a path

Table 3: Extensions of the tested samples – path of the bender 25 mm.

Material	DC05	HCT600X	AISI 304
Force [kN]	5.201 ± 0.105	10.453 ± 0.172	7.619 ± 0.133
Path of the bender in the loaded state h [mm]	25	25	25
The path of the bender in the unloaded state h' [mm]	23.55 ± 0.04	22.26 ± 0.08	22.15 ± 0.09
Angle α'' in the loaded state [°]	27.71	27.71	27.71
Angle α' in the unloaded state [°]	26.11	24.68	24.56
Free part length of the sample in the loaded state $2.X_0''$ [mm]	121.75	121.75	121.75
Free part length of the sample in the unloaded state $2.X_0'$ [mm]	120.440	119.33	119.241
The difference after unloading (springback) $X_0'' - X_0'$ [mm]	1.31	2.42	2.51
h – h'	1.45 ± 0.04	2.74 ± 0.08	2.85 ± 0.09

Table 4: Stiffness constant and measured deformation work at 3-point bending test with stretching.

Material		DC05 (ref)	HCT600X	AISI 304
Deformation work W_{def} [J] at the punch path	25 mm	65.1 ± 1.2	130.7 ± 2.0	95.3 ± 2.8
	fracture	246.3 ± 1.6	269.6 ± 2.1	620.1 ± 3.5
$W_{def} / W_{def\ ref}$		1.00	1.09	2.52
$W_{def\ 25mm} / W_{def\ 25mm\ ref}$		1.00	2.01	1.46
Stiffness constant c [N.m^{-1}]		0.207 ± 0.016	0.450 ± 0.012	0.324 ± 0.012
$c / c_{ref} = a / a_{ref}$		1.00	2.17	1.57
Note: (ref) – reference material				

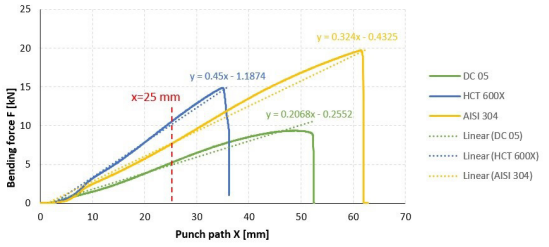

Figure 5: Record of the dependence of the bending force on the punch path (presented on single specimen for each material).

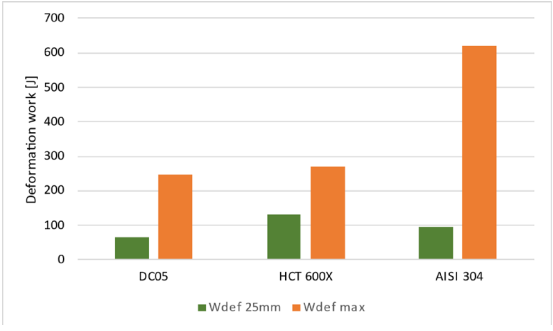

Figure 6: Comparison of average deformation work in 3-point bending with stretching .

of 25 mm (red vertical line), the HTC600X material is able to absorb the most energy.

When evaluating the interaction of bodies at impact, we will consider the balance of the interaction of forces (second Newton's law). It is possible to express the structure resistance by the stiffness constant c and deformation path as follows:

$$F_{max} = c \cdot x_{max}, \tag{4}$$

where F_{max} represents the maximum force value on the maximum deformation path xmax. From the action-reaction law it follows that at every moment of the collision, the resistance force of the structure FSV is equal to the multiple of the vehicle's weight and its acceleration:

$$F_{SV} = m \cdot a, \tag{5}$$

or

$$c_i \cdot x = m \cdot a_{i,max}, \tag{6}$$

If we consider that there will be a collision of vehicles with the same weight and the same geometry of deformation zones but made of different material, then it is possible to write the equation for a vehicle made of a reference material:

$$c_{ref} \cdot x = m \cdot a_{1,max}, \tag{7}$$

and for a vehicle structure made of a different material than the reference material:

$$c_i \cdot x = m \cdot a_{i,max}. \tag{8}$$

After comparing the deformation forces on the same path, we get the equation for the improvement ratio when changing the reference material to another:

$$\frac{a_{i,max}}{a_{max,ref}} = \frac{c_i}{c_{1,ref}}. \tag{9}$$

Equation (9) implies that the proportionality between the stiffness constants of the material under consideration and the reference material is directly related to the ratio of their body loads or decelerations. This means that we can estimate the amount of overload on a human in a vehicle collision depending on the stiffness constant of the material if we alter the material used to produce the deformation zones while keeping the same geometry and deformation path. It is important to make sure that there isn't an increase in overload with such a significant change. Thus, it is feasible to decrease a material's thickness while keeping the same deformation characteristics and simultaneously lowering the weight of the structure when employing a material with a greater stiffness constant.

4. Conclusions

The article focuses to the absorption characteristics evaluation for dual-phase steel HCT600X and austenitic steel AISI 304 (both with a nominal thickness of 0.8 mm) when compared to standard drawing quality steel DC 05. The deformation characteristics were evaluated by a three-point bending test with stretching. Based on the experiments and their evaluation, it can be stated:

– side impact - short deformation zone – path 25 – absorption potential is increased for HCT600X about 2.01x and AISI 304 about 1.46x;

– frontal impact – long deformation zone – up to fracture – absorption potential is increased for HCT600X about 1.09x and AISI 304 about 2.52x;

– the resistance of the material determined from the stiffness constant c of HCT600X when measured at the long path (up to the fracture) is 1.38x higher than that of AISI 304;

If the side deformation zone is considered, the deformation path is shorter than the deformation path in the front or rear zone. Thus, it would be appropriate to use HCT600X material, which absorbs almost twice as much energy on a 25 mm path compared to AISI 304 material. For the front and rear deformation zones, it is preferable to use AISI 304 material, which has been shown to absorb 2.3 times more energy than HCT600X material up to the point of fracture.

It was found that with the application of the stronger HCT600X material of the same thickness, there would be an increase in passenger overload at the same time. Therefore, in order to maintain the same level of overload, when applying a stronger material, it is necessary to reduce its thickness. The ideal choice of material for front deformation zones of the body in white would be AISI 304 austenitic steel, which, with a slightly increased value of the stiffness constant, provides us with a very good absorption potential. However, such steel is too expensive for application in the car structure, it could increase the price of the vehicle to such an extent that it would become unattractive for the consumer.

On the contrary, HCT600X steel, which has the ability to absorb a large amount of energy over a short distance, is suitable for side reinforcements where there is not enough space for the application of deformation elements that would absorb the impact over a sufficiently long distance. Therefore, when designing the deformation zones of the body, it is necessary to take into account many factors such as the path of deformation, the space required for the survival of the crew in the event of an impact, the magnitude of the overload and then find their balance. The right choice of material can save many lives and also save production costs for the manufacturer.

Acknowledgments

The work was done under the grant project VEGA 1/0238/23 "Implementation of CAx systems and virtual engineering techniques in the redesign of car-body parts for deformation zones".

References and Notes

1. Sun, C., Zheng, S., Ma, Y. et al. (2021) An active safety control method of collision avoidance for intelligent connected vehicle based on driving risk perception. Journal of Intelligent Manufacturing, Vol. 32, p. 1249–1269; doi: 10.1007/s10845-020-01605-x.
2. Čada, R. (1997) Formability of Deep-Drawing Steel Sheets. In: Proc. of Conference EUROMAT 97: Vol. 4 - Characterization and Production/Design. Netherlands Society for Materials Science, 1997, s. 463-466. ISBN 90-803513-4-2.
3. Moor, E. (2021) Advanced High-Strength Sheet Steels for Automotive Applications. High-Performance Ferrous Alloys, 1st ed., Springer Cham, Springer Nature Switzerland AG, 624 p., ISBN 978-3-030-53824-8. https://doi.org/10.1007/978-3-030-53825-5_4
4. Mihalikova, M., Német, M., Girman, V. (2015) DP600 Steel Research of Dynamic Testing. Metalurgija, Vol. 54, No. 1, p. 211-213.
5. Valeš, M., Novák, V., Tatíček, F., Šanovec, J., Chrášťanský, L. (2019) Outer car body panels made of dual-phase steel. Proceedings of the 28th Conference on Metallurgy and Materials, p. 507- 512.
6. Tolouei, R., Titheridge, H. (2009) Vehicle mass as a determinant of fuel consumption and secondary safety performance. Transportation Research Part D: Transport and Environment, Vol. 14, Issue 6, p. 385-399; doi.org/10.1016/j.trd.2009.01.005.
7. Fechová, E., Kmec, J. et al. (2016) Material Properties and Safety of Cars at Crash Tests. International Conference on Manufacturing Engineering and Materials, Vol. 149. p. 263-268; doi.org/10.1016/j.proeng.2016.06.665.
8. Németh S. (2014) Analysis of car safety in terms of the materials used in the deformation zones of the car body. In: Strojárstvo, vol. 7.
9. Gagliardi, F. et al. (2021) Environmental impact of material selection in a car body component – The side door intrusion beam. Journal of Cleaner Production, Vol 318, doi: 10.1016/j.jclepro.2021.128528.
10. Akhshik, M. et al. (2019) The effect of lightweighting on greenhouse gas emissions and life cycle energy for automotive composite parts. Journal of Clean Technologies and Environmental Policy., Vol. 21 Iss 3. p. 625-636; doi: 10.1007/s10098-018-01662-0.
11. Kubiak, P. (2018) Work of non-elastic deformation against the deformation ratio of the Subcompact Car Class using the variable correlation method. Forensic Science International, Vol. 287, p. 47-53; doi.org/10.1016/j.forsciint.2018.03.033.
12. Vlk, F. (2000) Karosérie motorových vozidel: ergonomika : biomechanika : pasivní bezpečnost : kolize : struktura : materiály. Brno: VLK, 2000. ISBN 80-238-5277-9.
13. Schwarz, T., Schritter, A., Köppel, T. et al. (2010) Active and passive safety, ATZextra Worldwide, Vol. 15, no. 5, p. 72-75; doi:10.1365/s40111-010-0203-1
14. Hasegawa, A., Egawa,Y et all. (2023) New load transfer

structure to reduce body deformation in side collisions. Traffic Injury Prevention, Volume 24, Supplement 1, p. S68-S74, ISSN 1538-9588, doi.org/10.1080/15389588.2022.2136944.

15. Pednekar, V., Pereira, A., Ballard, A., Chen, G. et al. (2020) Structural Performance Comparison between 980MPa Generation 3 Steel and Press Hardened Steel Applied in the Body-in-White A and B-Pillar Parts. SAE Technical Paper 2020-01-0537, https://doi.org/10.4271/2020-01-0537.
16. Rodríguez-Martínez, J.A., Rusinek, A., Pesci, R. (2010) Experimental survey on the behaviour of AISI 304 steel sheets subjected to perforation. Journal of Thin-Walled Structures., Vol. 48 Iss 12, p. 966-978; doi.org/10.1016/j.tws.2010.07.005.
17. Cotterell, M., Schambergerova, J. et al. (2002) Dependence of micro-hardness on deformation of deep-drawing steel sheets. Journal of Materials Processing Technology., Vol 124. Iss 3, p. 293-296; doi.org/10.1016/S0924-0136(02)00203-0.
18. Sommer, N., Lee, S. et al. (2023) Dynamic tensile deformation behavior of AISI 316L stainless steel fabricated by laser-beam directed energy deposition. Journal of Materials Research and Technology, Vol 27, p. 5896-5909; doi.org/10.1016/j.jmrt.2023.10.251.
19. Xu, P., Yang, C., Peng, Y., Yao, S., Zhang, D., Li, B. (2016) Crash performance and multi-objective optimization of a gradual energy absorbing structure for subway vehicles. Int. J. Mech. Sci. 2016, 107, 1–12.
20. Eroğlu, M. (2019) Advanced High Strength Steels (AHSSs): Production and Applications. Proceedings of the UDCS'19 Fourth International Iron and Steel Symposium, Karabuk University, Turey, Karabuk, 4–6 April 2019.
21. Larn, R.H.; Yang, J.R. (2000) The effect of compressive deformation of austenite on the bainitic ferrite transformation in Fe-Mn-Si-C steels. Mater. Sci. Eng. 2000, 278, 278–291.
22. International Organization for Standardization. (2019). Metallic materials - Tensile testing - Part 1: Method of test at room temperature. (ISO 6892-1:2019).
23. International Organization for Standardization. (2020). Metallic materials - Sheet and strip - Determination of plastic strain ratio. (ISO 10113:2020).
24. International Organization for Standardization. (2020). Metallic materials - Sheet and strip - Determination of tensile strain hardening exponent. (ISO 10275:2020).
25. Evin, E., Tomáš, M., Kmec, J. et al. (2014) The Deformation Properties of High Strength Steel Sheets for Auto-body Components. Procedia Engineering, Vol. 69, p.1-1568; https://doi.org/10.1016/j.proeng.2014.03.052